JOURNAL OF GEOPHYSICAL RESEARCH, VOL. 112, A11210, doi:10.1029/2007JA012416, 2007

Longitudinal and seasonal variations in plasmaspheric electron density: Implications for electron precipitation

M. A. Clilverd,[1] N. P. Meredith,[1] R. B. Horne,[1] S. A. Glauert,[1] R. R. Anderson,[2] N. R. Thomson,[3] F. W. Menk,[4] and B. R. Sandel[5]

Received 23 March 2007; revised 27 July 2007; accepted 15 August 2007; published 16 November 2007.

[1] The tilt and offset of the Earth's magnetic field can significantly affect the longitudinal and seasonal distribution of electron density in the plasmasphere. Here we show that for the solar maximum conditions of 1990–1991, the largest annual variation determined from CRRES measurements of plasmaspheric equatorial electron density in the range L = 2.5–5.0 occurs at American longitudes (−60°E), while no annual variation occurs at Asian longitudes (+100°E). Plasmaspheric electron density is larger in December than in June at most longitudes, from −180°E eastward to +20°E. At all other longitudes the density ratio from December to June is very close to 1.0. The largest December/June density ratio is at L = 3.0 at American longitudes (−60°E). At L = 4.5 and above, the annual variation disappears. The lowest electron density values for a given *L*-shell occur at American longitudes, in June. Ion densities also show significant annual variations, with similar longitudinal and seasonal characteristics in the case of IMAGE EUV He^+ measurements. Atomic mass density measurements calculated using the magnetometer cross-phase technique show significant seasonal variations but also imply composition changes with longitude. Using the quasilinear PADIE code we calculate the bounce-averaged diffusion rate of electrons by plasmaspheric hiss with a fixed wave intensity. December to June variations in plasmaspheric density, particularly at American longitudes, drive changes in the wave-particle interactions, increasing diffusion into the loss cone by a factor of ∼3 at 1 MeV at L = 3.0, thus hardening the electron precipitation spectrum during the southern hemisphere winter (in June).

Citation: Clilverd, M. A., N. P. Meredith, R. B. Horne, S. A. Glauert, R. R. Anderson, N. R. Thomson, F. W. Menk, and B. R. Sandel (2007), Longitudinal and seasonal variations in plasmaspheric electron density: Implications for electron precipitation, *J. Geophys. Res.*, *112*, A11210, doi:10.1029/2007JA012416.

1. Introduction

[2] The plasmasphere is a region of low-energy ("cold," i.e., T_e ∼1 eV) plasma surrounding the Earth, and extending out to L ∼2–6 depending on geomagnetic latitude, geomagnetic disturbance levels, and on local time. It is primarily made up of electrons and protons that have diffusively migrated from the underlying ionosphere. Overlapping the plasmasphere are regions of high-energy ("hot," i.e., T_e ∼ 1 MeV) plasma known as the radiation belts. Low-frequency radio waves propagating within the plasmasphere can interact with the high-energy radiation belt particles, changing their energy spectra and causing them to precipitate into the Earth's upper atmosphere, driving chemical changes [e.g., *Rozanov et al.*, 2005]. Variability in the background conditions of the plasmasphere is one of the factors in determining the efficiency of wave-particle interactions [e.g., *Horne et al.*, 2003], thus influencing the resultant particle precipitation into the atmosphere. Here we use CRRES satellite measurements of "cold" plasmaspheric equatorial electron density to investigate the longitudinal and annual variations in density in the range L = 2.5–5.0, and assess the effect on the rate of "hot" electron precipitation from the overlapping outer radiation belt.

[3] The annual variation in equatorial plasmaspheric electron density (Neq) has been observed previously. The first observations were made using natural whistler signals, typically at either American or European longitudes [e.g., *Helliwell*, 1965; *Park et al.*, 1978; *Tarcsai et al.*, 1988]. In these cases Neq showed a maximum in December and a minimum in June, with December larger by a factor of between 1.5 and 3.0 at L = 1.5–2.5, depending on longitude.

[4] Man-made whistler-mode signals from US Naval transmitters were analyzed by *Clilverd et al.* [1991] and showed a December to June ratio of Neq of 3.0 (2.0) at solar minimum (maximum) at L = 2.5 in the American longitude

[1]British Antarctic Survey, Natural Environment Research Council, Cambridge, UK.
[2]Department of Physics and Astronomy, University of Iowa, Iowa City, Iowa, USA.
[3]Department of Physics, University of Otago, Dunedin, New Zealand.
[4]Department of Physics, University of Newcastle, Newcastle, Australia.
[5]Lunar and Planetary Laboratory, University of Arizona, Tucson, Arizona, USA.

0148-0227/07/2007JA012416$09.00

sector, and a ratio of 1.4 at solar maximum in the New Zealand/Pacific longitude sector. Using conjugate ionosonde pairs such as Wallops Island (37.9°N, 75.5°W, L = 2.39) and Argentine Islands (65.3°S, 64.3°W, L = 2.44), *Clilverd et al.* [1991] showed that the seasonal Neq variation was largest at 300°E geographic (−60°E) because at that longitude the offset of the geomagnetic field configuration relative to geographic coordinates is largest. Calculations showed that each field line flux tube is in long-term diffusive equilibrium with the underlying ionospheres at the footprints of the field line and the annual behavior of the plasmasphere reflects the local annual variation of the northern and southern F2 regions linked to it. In Figure 1 we show this variation of the geographic latitude of the footprints of the L = 2.5 field line contour, using the IGRF magnetic field model, as a function of geographic longitude. The southern L = 2.5 contour at −60°E has an underlying ionosphere that is at high latitude and thus continually sunlit during the December solstice, and in near-continuous darkness during the June solstice. These factors, along with differing horizontal thermospheric winds at such high geographic latitudes driving the ionospheric plasma up the field lines, produce significant changes in plasmaspheric density from solstice to solstice. *Clilverd et al.* [1991] also suggested that there would be no annual variation at African/Asian longitudes, and that in June global Neq values at L = 2.5 would be largely independent of longitude and similar to that observed at −60°E, that is, ∼1000 el cm^{-3}.

[5] The annual variation in Neq has been modeled with a view to reproducing the observations and understanding the underlying physical processes responsible. Some models reproduced the December/June annual variation at American longitudes, and then made predictions regarding the effect at other longitudes. Early work by *Rasmussen and Shunk* [1990] showed a Neq maximum in June rather than December as is actually observed, probably because of the centered dipole model used. Modeling work undertaken by *Rippeth et al.* [1991], which included a tilted offset dipole in the model, was better able to reproduce the observations at L = 2.5 at American longitudes. *Guiter et al.* [1995] modeled plasmaspheric densities at L = 2 and found that Neq was 1.5 times higher in December than in June for 300°E (−60°E) longitude. At 120°E longitude the L = 2 Neq was predicted to be higher in June than December by a factor of 1.2. The underlying mechanism driving the annual variation was considered to be variations in ionospheric O^+.

[6] Further modeling using the field line interhemispheric model (FLIP) indicated that the annual variation at American and Australian longitude sectors were likely to be 6 months out of phase [*Richards et al.*, 2000]. This work concluded that plasmaspheric thermal structure, not ionospheric density, should play a key role in producing the annual variation at solar minimum. A new approach using dynamical diffusive equilibrium, called the global plasmasphere ionosphere density model (GPID), was able to reproduce the observed seasonal variations in Neq at L = 2.5 during solar maximum, but not at solar minimum [*Webb and Essex*, 2001].

[7] To maintain charge neutrality an annual variation in ion concentration would be anticipated. *Berube et al.* [2003] used data from a pair of magnetometers at L = 1.74 in the MEASURE array (American longitudes) to determine the plasmapsheric equatorial mass density. They observed an annual variation in mass density with December densities 2–3 times higher than in June. This suggests that the mass densities vary in a similar way to the electron densities. Although at L < 2, the annual variation in field line resonance frequencies is due to the influence of O^+ in the underlying ionosphere changing the Alfven speed profile along those flux tubes [*Waters et al.*, 1994].

[8] Here we perform a comprehensive study of the longitudinal and seasonal variation of the equatorial plasmaspheric electron density in the region 2.5 < L < 5.0 using data from the CRRES satellite. We examine the observed Neq radial profiles during solar maximum conditions (1990/1991) at different longitudes and at different times of year, and compare the profiles against the commonly used profiles of *Carpenter and Anderson* [1992]. We also investigate the equivalent mass density variations using the IMAGE EUV measurements of He^+, and atomic mass from the cross-phase analysis of ground-based magnetometer data. The relevance of the plasmaspheric density variations are put into the context of changing wave-particle interactions, and the subsequent deposition of energetic particles into the upper atmosphere.

2. Determination of Electron Densities in the Plasmasphere

[9] Electron number densities are derived from wave data provided by the Plasma Wave Experiment on board the Combined Release and Radiation Effects Satellite (CRRES). This satellite, which was launched on 25 July 1990, operated in a highly elliptical geosynchronous transfer orbit with a perigee of 305 km, an apogee of 35,768 km and an inclination of 18°. The orbital period was approximately 10 h, and the initial apogee was at a magnetic local time (MLT) of 0800 MLT. The magnetic local time of apogee decreased at a rate of approximately 1.3 h per month until the satellite failed on 11 October 1991, when its apogee was at about 1400 MLT. The satellite swept through the plasmasphere on average approximately 5 times per day for almost 15 months. The Plasma Wave Experiment provided measurements of electric fields from 5.6 Hz to 400 kHz, using a 100 m tip-to-tip long wire antenna, with a dynamic range covering a factor of at least 10^5 in amplitude [*Anderson et al.*, 1992].

[10] The sweep frequency receiver, which is used in this study, covered the frequency range from 100 Hz to 400 kHz in four bands with 32 logarithmically spaced steps per band, the fractional step separation being about 6.7% across the entire frequency range. Band 1 (100 Hz to 810 Hz) was sampled at one step per second with a complete cycle time of 32.768 s. Band 2 (810 Hz to 6.4 kHz) was sampled at two steps per second with a complete cycle time of 16.384 s. Band 3 (6.4 to 51.7 kHz) and band 4 (51.7 kHz to 400 kHz) were sampled 4 times per second with complete cycling times of 8.192 s.

[11] The electron number density is determined from the electron plasma frequency, fpe, using the standard expression $n_e = 4\pi^2 f_{pe}^2 \varepsilon_0 m_e / e^2$. When emissions at the upper hybrid frequency, f_{uhr}, are well-defined the electron plasma frequency, f_{pe}, is derived from f_{uhr} using the relationship $f_{pe}^2 =$

$f_{uhr}^2 - f_{ce}^2$, where f_{ce} is the electron gyrofrequency, determined from the CRRES fluxgate magnetometer [*Singer et al.*, 1992]. When the upper hybrid frequency cannot be identified the electron plasma frequency is estimated from the lower-frequency limit of the electromagnetic continuum radiation, which is taken to be the plasma wave cutoff at the plasma frequency [*Gurnett and Shaw*, 1973]. The number densities are initially determined at a temporal resolution of 8.192 s and subsequently averaged as a function of half orbit (inbound or outbound) and L in steps of 0.1 L. The position of the CRRES spacecraft is mapped to the ionosphere at the same temporal resolution using the IGRF 85 model corrected for external magnetospheric currents by the Olson-Pfitzer tilt dependent static model [*Olson and Pfitzer*, 1977]. This is the standard process used to analyze all CRRES data. The geographic coordinates are then averaged as a function of half orbit and L shell in steps of 0.1 L. The time in UT, magnetic latitude, magnetic local time, and time spent in each bin are also recorded at the same resolution.

[12] The resulting database is subsequently analyzed to determine the behavior of the plasmaspheric equatorial number density as a function of geographic longitude and for different *L* shells and seasons. Throughout this paper we use geographic longitude during discussions of the results and the figures shown. We focus on periods centered near the solstices and use the data from October to February (inclusive) for the December solstice and from April to August (inclusive) for the June solstice. For each season the data are averaged into bins that are 5° in geographic longitude for *L* shells ranging from 2.5 ± 0.3 L to 5.0 ± 0.3 L in steps of 0.5 L. The data are included in the averaging process only when the measurements are made within the plasmasphere and when the magnetic latitude of the CRRES spacecraft lies within ±10° of the magnetic equator.

[13] Data are selected to be in the plasmasphere using a criterion based on the amplitude of the waves in the frequency band $f_{ce} < f < 2f_{ce}$. Waves in this frequency band, which contains contributions from both electron cyclotron harmonic waves and thermal noise, tend to be excluded from the high density region inside the plasmapause. Specifically observations in the plasmasphere are identified using the criterion that the wave amplitude for frequencies in the range $f_{ce} < f < 2f_{ce}$ must be less than 0.0005 mVm^{-1} [*Meredith et al.*, 2004]. Observations made in regions where this criterion did not hold are assumed to be outside the plasmapause at the time and are excluded from the analysis. In practice although we exclude data during large geomagnetic storms using the wave amplitude criterion we will include some density values when the plasmasphere is likely to be in an intermediate refilling state following the storms. Overall, our criterion for selecting plasmaspheric measurements is somewhat conservative in that we reject ~14% of the data where the ECH waves in the range $f_{ce} < f < 2f_{ce}$ have amplitudes above 0.0005 mV m^{-1} but the densities are likely to be representative of the plasmashere at the time [*Meredith et al.*, 2004]. However, this criterion does reduce the number of low density measurements included in our analysis where the plasmapause is ill-defined, and when the plasmasphere is subject to erosion during geomagnetically active periods (i.e., AE > 100 nT).

3. Determination of Ion Densities in the Plasmasphere

[14] The ion mass densities presented in this study were calculated using field-line resonant frequencies (FLRs) measured from pairs of ground-based magnetometers, following the analytical expressions described by *Taylor and Walker* [1984] and *Walker et al.* [1992]. These assume decoupled toroidal mode oscillations and yield essentially identical results to the models described by *Orr and Matthew* [1971]. Techniques for the detection of FLRs were summarized by *Menk et al.* [1999] and *Menk et al.* [2000]. When examining data from latitudinally separated magnetometers, the resonant frequency is identified by the peak in H-component cross-power and cross-phase, and a unity crossing in H-component power ratio, approximately midway between the stations. Where only one station is available the resonance is indicated by a peak in the power ratio H/D and a rapid change in polarization, that is, in the phase between the H and D components.

[15] The uncertainty in our calculated mass densities presented in this study (20–30%) depends mainly on uncertainty in the frequency measurement with uncertainties typically of order 10–15%. *Menk et al.* [1999] discussed the relationship between these two uncertainties and found the mass density uncertainty to be typically double the uncertainty in frequency measurement. We have assumed a dipole magnetic field, and at L = 2.5 this introduces negligible error.

[16] Measurements of the He^+ ion density presented in this study were made with the Extreme Ultraviolet Imager (EUV Imager) on board the IMAGE spacecraft, by detecting its resonantly scattered emission at 30.4 nm [*Sandel et al.*, 2001]. The IMAGE spacecraft is in an elliptical polar orbit with an apogee altitude of 7.2 Earth radii (46,000 km) and a perigee altitude of 1,000 km, and completes one orbit every 14.2 h. Effective imaging of the plasmaspheric He^+ requires global "snapshots" in which the high apogee and the wide field of view of the EUV Imager provide in a single exposure a map of the entire plasmasphere. The 30.4 nm feature is relatively easy to measure because it is the brightest ion emission from the plasmasphere, it is spectrally isolated, and the background at that wavelength is negligible. Line-of-sight measurements are easy to interpret because the plasmaspheric He^+ emission is optically thin, so its brightness is directly proportional to the He^+ column abundance. The EUV Imager instrument consists of three identical sensor heads, each having a field of view of 30°. These sensors are tilted relative to one another to cover a fan-shaped field of 84° × 30° that is swept across the plasmasphere by the spin of the satellite. EUV Imager's spatial resolution is ~0.6° or ~0.1 Re in the equatorial plane seen from apogee. The sensitivity is sufficient to map the position of the plasmapause with a time resolution of 10 min or better.

[17] For this study we selected EUV measurements from times in June and December 2001. We used 122 images taken from the period 15–17 June and 97 images from the period 9–20 December. All images were from quiet times

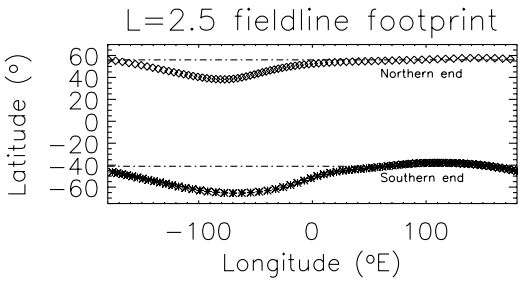

Figure 1. Variation of the geographic latitudes of the footprints of the L = 2.5 field line, showing significant changes in relative latitude in the longitude region of −60°E.

(Kp ≤ 2), chosen to avoid azimuthal structures that often appear during more active times. After transforming each image to the plane of the magnetic equator [*Sandel et al.*, 2003] using magnetic longitude as the azimuthal coordinate, we summed the images to a single image for each of June and December. The summation omitted the region of Earth's shadow and the overlaps between the three EUV cameras.

[18] We derived azimuthal profiles of brightness versus magnetic longitude by sampling these composite images in an annulus of width 0.3 L centered at L = 2.5 with a bin size of 5° in magnetic longitude. To infer equatorial He^+ abundances from the measured brightness, we used the concept of effective path length described by *Clilverd et al.* [2003] and *Gallagher et al.* [2005].

4. Longitudinal and Seasonal Variations in Plasmaspheric Densities

[19] Figure 2 shows the density variation with longitude from CRRES for December (solid line) and June (dashed line) for L = 2.5–5.0. Some of the data shown for December at L = 2.5 are indicated by a dot-dashed line, indicating that they are less reliable than the other data. The densities at these longitudes in December were so large (>2000 el. cm^{-3}) that the upper hybrid frequency could not be determined at all times, and data from a higher range of *L*-shells (L = 2.7–3.3) were used and linearly extrapolated to L = 2.5 and shown as the dot-dashed line. Thus the data should be treated as less reliable than the rest shown. However, the same extrapolation technique used on the L = 2.5 June data, and some of the other panels (L = 3.0–4.0) reproduced the December data to within 5%. We make this extrapolation for the L = 2.5 December data primarily to allow comparison with previous work, it does not materially affect any of the conclusions from this paper.

[20] For L = 2.5–3.5 it is clear that the density is much higher in December than June over the longitude range −180°E to 20°E. At the remaining longitudes the December and June densities are much more nearly equal, with occasionally the June densities exceeding the December ones by up to 10%. The same relationship occurs for the higher *L*-shell regions (L ∼ 4.0), although the data are more sparse because of incursions by the plasmapause and hence the plots are somewhat less clear. As expected the average density level decreases with increasing *L*-shell as the plasma from the underlying ionosphere diffuses up into ever increasing flux tube volumes. This is true for each season, and every longitude.

[21] The largest difference in density between December and June occurs at about −60°E longitude, which is consistent with the conclusions of *Clilverd et al.* [1991]. At L = 2.5 the densities in June at this longitude are ∼1000 el.cm^{-3}, while the December densities are ∼2500 el.cm^{-3}. This compares well with the whistler-mode results shown in the work of *Clilverd et al.* [1991] which were 1400 el.cm^{-3} and ∼2800 el.cm^{-3} respectively in June and December, at solar maximum. The 10–40% systematically higher results from the whistler-mode signals may be due to a slightly lower average *L*-shell than L = 2.5, i.e., L = 2.45 [*Saxton and Smith*, 1989]. If the average whistler-mode *L*-shell used by *Clilverd et al.* [1991] is 0.05 L equatorward of L = 2.5 this would make only an 8% difference to the electron density calculations. The extrapolation error of 5% should also be included in this interpretation, suggesting that ∼10% of the difference between the two techniques could be due to errors in assumptions made. The remainder may be due to the requirement for whistler-mode signals to propagate in field-aligned electron density enhancements and suggest that duct enhancements maybe typically 20% of the average electron density levels, in agreement with previous ray-tracing calculations of 10–20% [*Strangeways*, 1991].

[22] The change in the annual variation of Neq with *L*-shell is shown in Figure 3 as a ratio of December to June Neq values. Three longitudes are shown, +100° (Asia), −60° (America), and −150° (New Zealand). While not actually at the exact longitude of New Zealand, the longitude (−150°) is used because it is the appropriate longitude for the "New Zealand" ground-based whistler-mode data [*Clilverd et al.*, 1992] which showed an annual variation ratio of ∼1.4. At Asian longitudes there is virtually no annual variation, with the Neq ratio staying within ±10% of unity. The American longitudes show a maximum ratio of 2.7 at L = 2.5–3.5. By L = 4.5 the annual variation in Neq has almost disappeared. The New Zealand longitudes show a relatively small annual variation, with a ratio of about 1.5, with a gradual decline in the effect with increasing *L*-shell.

[23] The radial density profile in the plasmasphere is typically represented as an L^{-4} distribution. The following expression based on the plasmaspheric model of *Chappell et al.* [1970] is used to represent the results obtained from whistler-mode signals:

$$N_{eq} = 3877 P_e^2 [2/L]^N \quad \text{el.cm}^{-3} \qquad (1)$$

where P_e is a plasma enhancement factor, usually taken as 1.0, N is the radial power law, usually assumed to be 4.0, and 3877 el.cm^{-3} is the electron density at L = 2.0. The results of least squares fitting of equation (1) to the data for both +100°E (Asia) and −60°E (American) longitudes in December and June is shown in Figure 4. The values of P_e and N are shown in each panel, with the best fit represented by a solid line. The Neq data points are shown by diamonds. A dotted reference line using the empirical Carpenter and Anderson plasmasphere model [*Carpenter and Anderson*, 1992] for December and June during solar maximum conditions (sunspot number, R = 150) is also shown. The

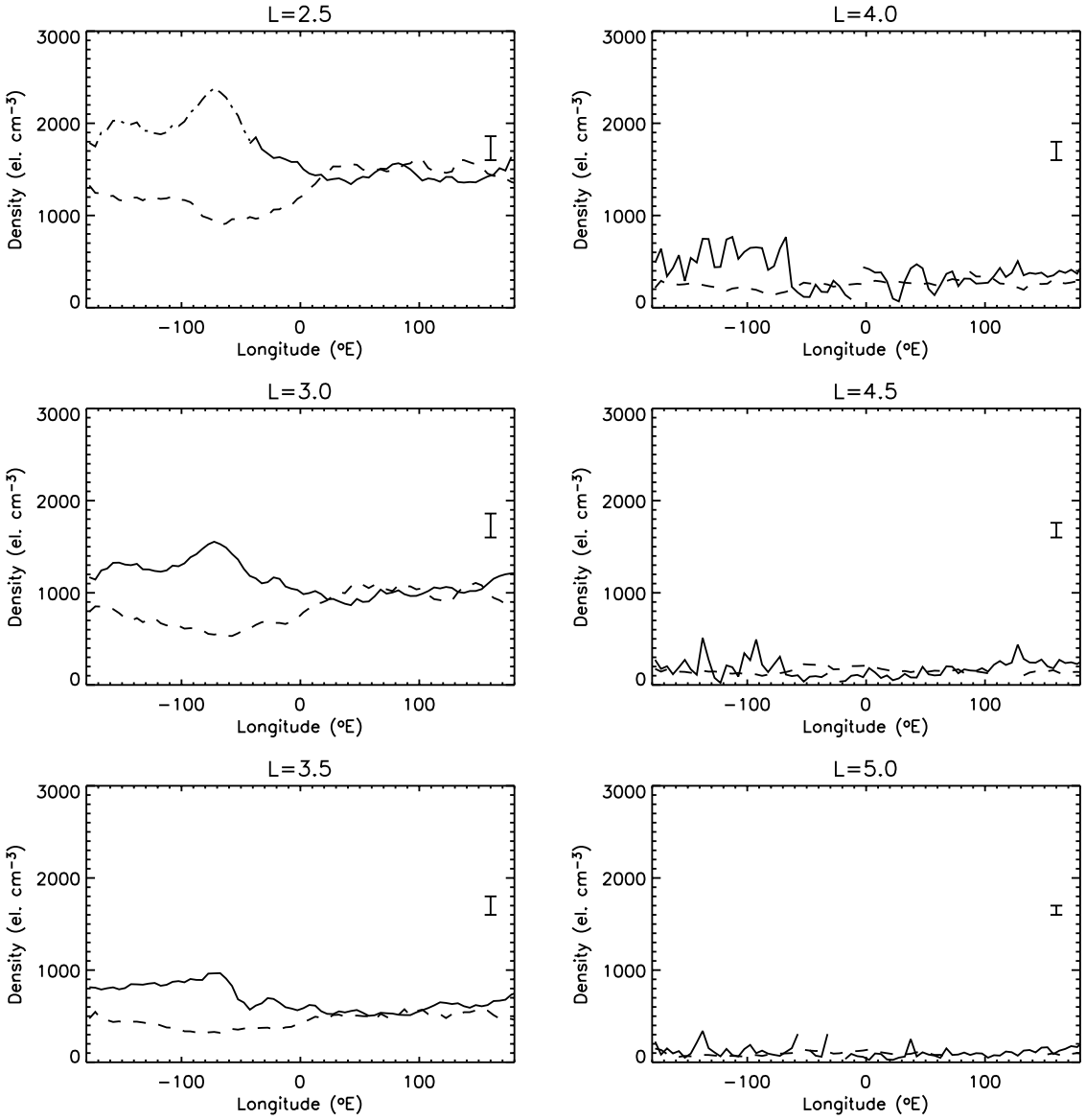

Figure 2. Longitudinal variation of equatorial electron density from the CRRES data plotted for a range of *L*-shells. Data from the December solstice (solid lines) are compared with data from the June solstice (dashed line). An error bar is shown representing one standard deviation in the data.

Carpenter and Anderson model was developed from satellite profiles of N_{eq} that included coverage at $L \leq 3$, and restricted to those profiles where $N_{eq} > 667$ el.cm^{-3} at L = 3. Profiles were then used until they became irregular at higher *L*-shells or exhibited a steeper negative slope. This, and the requirement that geomagnetic activity had been low for ~20 h prior to the profile measurement, ensured that the model represents the quiet-time, saturated plasmasphere. However, the CRRES results shown in Figure 2 suggest that these electron density restriction at L = 3 would reject some saturated plasmasphere conditions found at American longitudes around the time of the June solstice. We would expect our ECH limitation on the CRRES data selection to ensure saturated plasmasphere measurements, but potentially only at *L*-shells which are typically unaffected by weak or moderate geomagnetic activity (L < 4).

[24] In Figure 4 the CRRES data for Asian longitudes (+100°E) show little variation with season, with P_e and N values very close to the normal values used, that is, 1.0 and 4, respectively. At American longitudes (−60°E) there are significant changes in the radial profile from December to June. In December the best fit is given by $P_e = 1.6$ and N = 5. So the $L \leq 3$ density levels are elevated compared with normal values and the radial profile is steeper than expected. In June $P_e = 0.75$, and N = 3.4 and the densities are lower than normal, and the radial profile is less steep. Averaged over longitude at any given time of year the density profiles should look similar to those given by Carpenter and Anderson because their analysis did not take longitudinal variability into account. In practice this is true for our data until L > 3.5, after which the consistently lower densities seen in our data shows clear evidence that our analysis

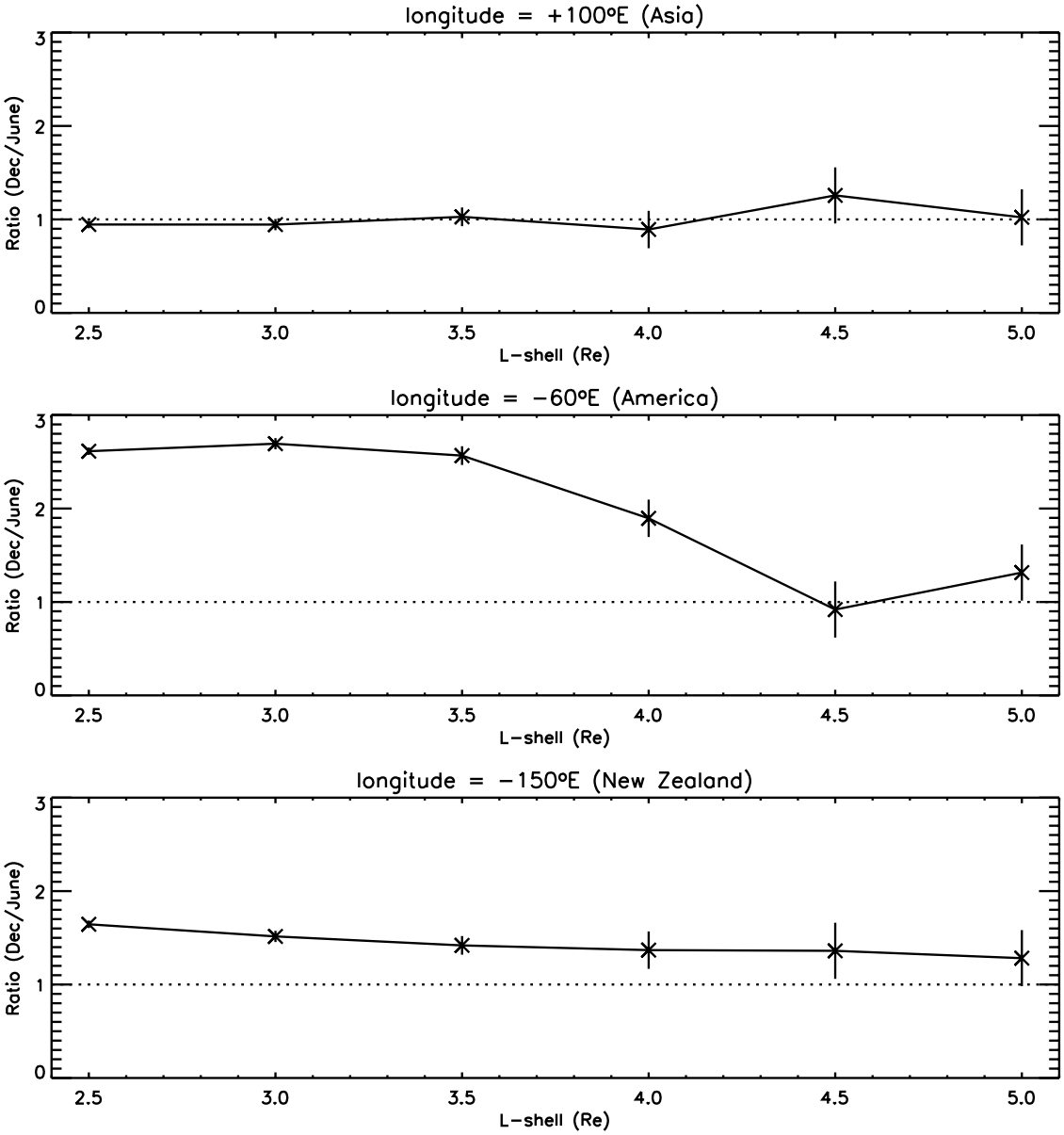

Figure 3. Variation of the December/June ratio with *L*-shell, at the longitudes of Asia, America, and New Zealand/Pacific, derived from the CRRES data.

includes some nonsaturated density levels, that would have been excluded from the Carpenter and Anderson model.

[25] The annual variation in electron density should be mirrored in the ion density in order to conserve charge neutrality in the plasmasphere. In Figure 5 we plot the longitudinal and seasonal variation of He^+ abundance derived from the IMAGE EUV experiment [*Sandel et al.*, 2001]. The EUV units are He^+ (cm^{-3}), and are taken from measurements made in June and December 2001. The December EUV values are represented by crosses, with June values by diamonds. The longitudinal variations in He^+ closely match the electron density variations despite being taken from different solar cycles.

[26] To avoid a bias introduced by the diurnal variation in ion abundance, we aimed to select times for which the phase of the magnetic longitude system was uniformly distributed in magnetic local time. The final set of images chosen was imperfect in this regard. Therefore we assessed the possibility that some of the structure in the EUV measurements in Figure 5 could arise from incomplete averaging of the diurnal variation over all magnetic longitudes. We created a simple model to compute the residual modulation in magnetic longitude that might result from our specific sampling of the diurnal variation. It showed a modulation of lower amplitude, having a shape different from the structure in Figure 5. We conclude that imperfect averaging of the diurnal variation does not significantly bias the structure measured in longitude.

[27] Ion number densities have been calculated for Figure 5 using cross-phase analysis [*Menk et al.*, 1999] for the

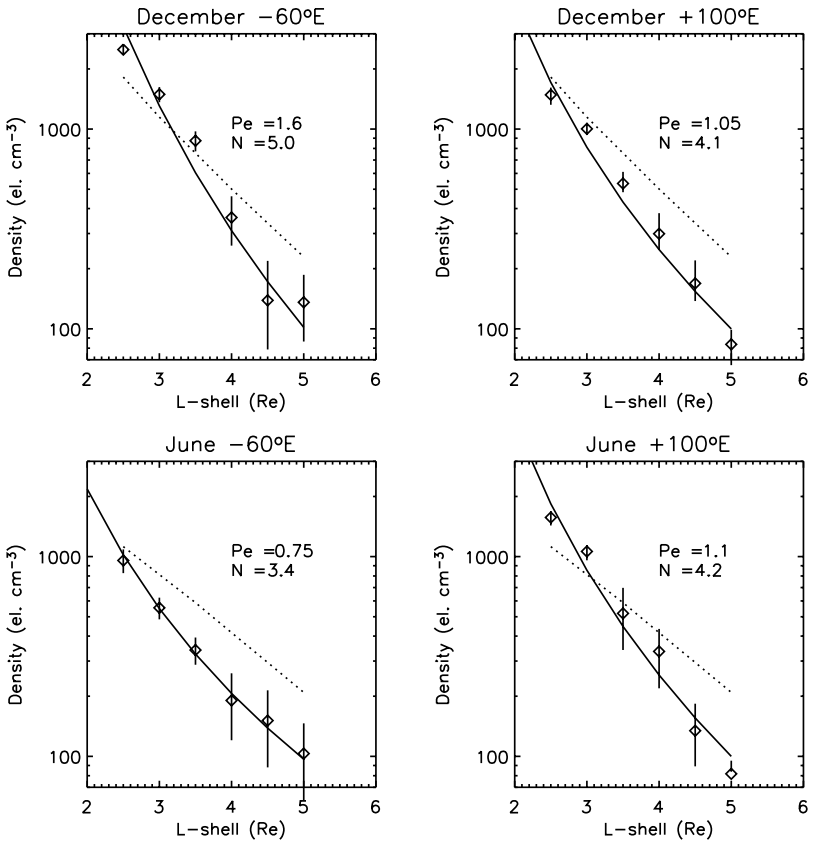

Figure 4. Radial profile of equatorial electron densities from CRRES data for a range of *L*-shells and longitudes (diamonds). Standard deviations for the data are shown. A fit to the data is given by the solid line, expressed in terms of Pe and N from equation (1). The *Carpenter and Anderson* [1992] model results for solar maximum conditions and low magnetic activity are also shown (dotted lines).

longitudes of −65°E and −10°E at L = 2.5 for December/June 2001. These data are shown in Figure 5 as squares (December) and triangles (June), and also indicate a strong annual variation in density at the longitudes observed. The pair of magnetometer stations used for the −65°E values is Millstone Hill and APL from the MEASURE array, and the −10°E values are Hartland and York from the SAMNET array. Both midpoints are close to L = 2.5, but have been normalized to exactly L = 2.5 assuming a radial L^{-4} variation. The ion values plotted at −65°E have been adjusted by a factor of 1.3 in order to convert atomic mass units to number densities and to make the plotted points match the electron densities at that longitude. The adjustment value suggests 11% composition of He^+ and the EUV data suggest ∼20%. These results are consistent with the H^+/He^+ composition during quiet times. Environmental differences due to different sampling times, and differences due to different techniques may be adequate to account for the differences observed here. However, the ion values at −10°E have been adjusted by a factor of 2.1. Although the data clearly shows the annual variation in density, the adjustment factor is much larger than expected and is consistent with significant heavy ion loading at these longitudes, that is, about 6% O^+. However, this result is not inconsistent with the results from *Sutcliffe et al.* [1987] who found increasing plasma mass density with longitude eastwards towards 20°E in June at L ∼ 1.78, due to increased O^+ concentrations at 1000 km, probably driven by vertical ion drifts from meridional winds in the upper ionosphere.

5. Implications for Electron Precipitation

[28] The background electron density in the plasmasphere plays a key role in determining the resonant energy of wave-particle interactions. In this section we investigate the influence that the annual variation in electron density will have on pitch-angle scattering of energetic electrons into the loss cone, out of the radiation belts, and subsequent precipitation into the atmosphere.

[29] *Meredith et al.* [2006] calculated loss timescales for pitch angle scattering by plasmaspheric hiss using the PADIE code [*Glauert and Horne*, 2005] with wave properties based on CRRES observations. The determination of the diffusion coefficients requires knowledge of the distribution of the wave power spectral density with frequency and wave normal angle, together with the ratio fpe/fce, wave mode, and the number of resonances. The ratio fpe/fce is dependent on the background electron density, and the background magnetic field.

[30] Here we analyze the effect of differing levels of plasmaspheric density at L = 3.0 using the PADIE code. Following the analysis of *Meredith et al.* [2006], we use similar parameters to model the wave interactions. Since

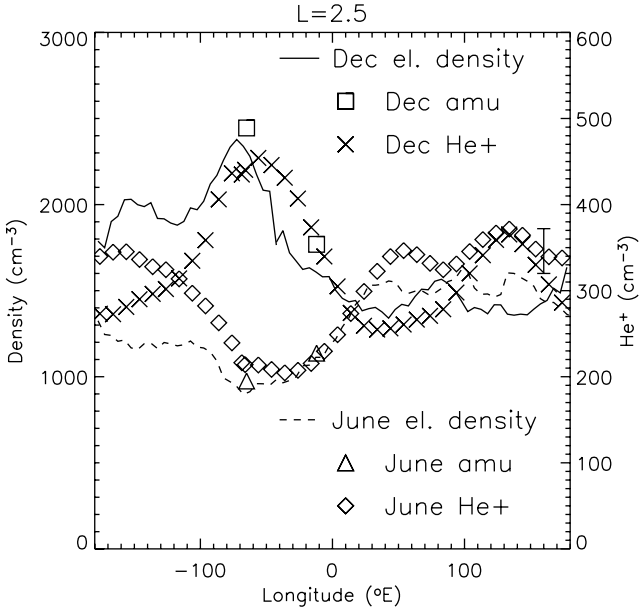

Figure 5. CRRES equatorial electron density variation with longitude at L = 2.5 for December (solid line) and June (dashed line). The longitudinal variation of IMAGE EUV He^+ abundances in 2001 for December (crosses) and June (diamonds) are shown in comparison, using the right-hand y-scale). Ion number densities from ground-based cross-phase techniques are shown for December (squares) 2003 and June 2001 (triangles) using the atomic mass unit adjusted by a weighting factor; see text for more details.

energetic outer zone electron loss timescales inside the plasmasphere can be explained by wave particle interactions with plasmaspheric hiss propagating at small or intermediate wave normal angles (ψ), we assume a Gaussian angular spread in X, where X = tan ψ, with a width corresponding to ψ = 20°. Since wave propagation at an angle to B is included, we calculate the diffusion rates for Landau (n = 0) and ±10 cyclotron harmonic resonances. We assume a wave power of 900 pT^2 and that the wave spectra intensity peaks at 0.55 kHz, with a bandwidth of 0.3 kHz and lower and upper cut-offs of 0.1 kHz and 2.0 kHz, respectively. Following *Lyons et al.* [1972], we calculate the bounce-averaged diffusion rate which takes into account the scattering of particles in pitch angle over the complete range of latitudes between the mirror points.

[31] We use values of the ratio fpe/fce that are equivalent to electron density levels of 1500 el.cm^{-3} (fpe/fce = 10.8), 1000 el.cm^{-3} (fpe/fce = 8.8), and 500 el.cm^{-3} (fpe/fce = 6.2). The PADIE code assumes a dipole magnetic field, and we use values of fpe/fce that are calculated at the L = 3.0 geomagnetic equator. These density levels represent conditions at L = 3.0 for American longitudes in December (1500 el.cm^{-3}) and June (500 el.cm^{-3}) taken from Figure 2, and the Asian longitudes for most times of the year (1000 el.cm^{-3}). The pitch angle diffusion coefficients are shown in Figure 6. The fpe/fce conditions are shown, with the bounce-averaged diffusion coefficient ($\langle D_{\alpha\alpha}\rangle$) plotted against electron pitch angle for three different electron energies. At times the bounce-averaged diffusion coefficient becomes extremely small and lies off the plot for large ranges of pitch angle. The 100 keV results for pitch angles <65° (long dashed line) during low plasmaspheric density conditions (fpe/fce = 6.2) is an example. The plot shows that for 100 keV electrons the diffusion rate at the edge of the loss cone (vertical dot-dashed line at pitch angles of ~10°) is reduced by a factor of ~5 as the plasmasphere becomes depleted to density levels equivalent of American longitudes around the June solstice. However, 1 MeV electron diffusion rates increase by a factor of ~3. Thus between December and June hiss driven precipitation into the atmosphere will become spectrally harder at American longitudes. At Asian longitudes, represented by fpe/fce = 8.8, there would be little change in the precipitation particle energy spectra with season since fpe/fce hardly changes.

6. Discussion

[32] Using CRRES observations set we have shown that the maximum amplitude of the annual variation in electron density is at American longitudes (about −60°E). This is in good agreement with the analysis of *Clilverd et al.* [1991], and it seems very likely that this is primarily caused by the influence of the Earth's tilted-offset dipole magnetic field on the diffusive equilibrium conditions along the plasmaspheric field lines, as represented by Figure 1 of this paper. The annual variation has an amplitude of 2.7 at L = 2.5 at solar maximum for American longitudes, which agrees with the corresponding densities derived from ground-based observations of whistler-mode signals. At New Zealand longitudes the ratio from CRRES observations was 1.5 for L = 2.5, which is also very close to the value found from whistler-mode signals taken during the same period.

[33] Several of the plasmaspheric models predicted that at Asian longitudes (+100°E) the June densities would exceed the December densities, by typically a ratio of 1.2 [*Guiter et al.*, 1995; *Richards et al.*, 2000]. This result is not observed in the CRRES data, where the ratio is 1.0 at almost all of the *L*-shells at this longitude. *Guiter et al.* [1995] predicted that the December to June density ratio would increase slightly with increasing *L*-shell. This is not observed at any of the longitudes studied in detail.

[34] The CRRES data shows that the June electron density levels at American longitudes are lower than for any other longitude. *Clilverd et al.* [1991] suggested that in June there would be very little longitudinal variation in electron density, and estimated Asian June density levels of 1000 el.cm^{-3}. This estimate was based on conjugate pairs of ionosonde data, since no suitable whistler-mode data was available for the Asian sector. For the African/Asian longitudes Nurmijarvi (60.5°N, 24.6°E) and Kerguelen (49.4°S, 70.2°E) were analyzed, mainly because of the lack of choice of ionosonde stations in the southern hemisphere at these longitudes. These stations represent L = 3.0–3.5 conditions rather than L = 2.5, and Figure 2 shows that typical Asian electron density levels at these L-shells of ~3.0 are ~1000 el.cm-3, thus explaining how the Asian sector equatorial electron density estimates of *Clilverd et al.* [1991] were too low. The longitudinal variation of Neq in June, although not previously predicted, is consistent with a tilted offset dipole magnetic field effect on plasmaspheric diffusive equilibrium conditions.

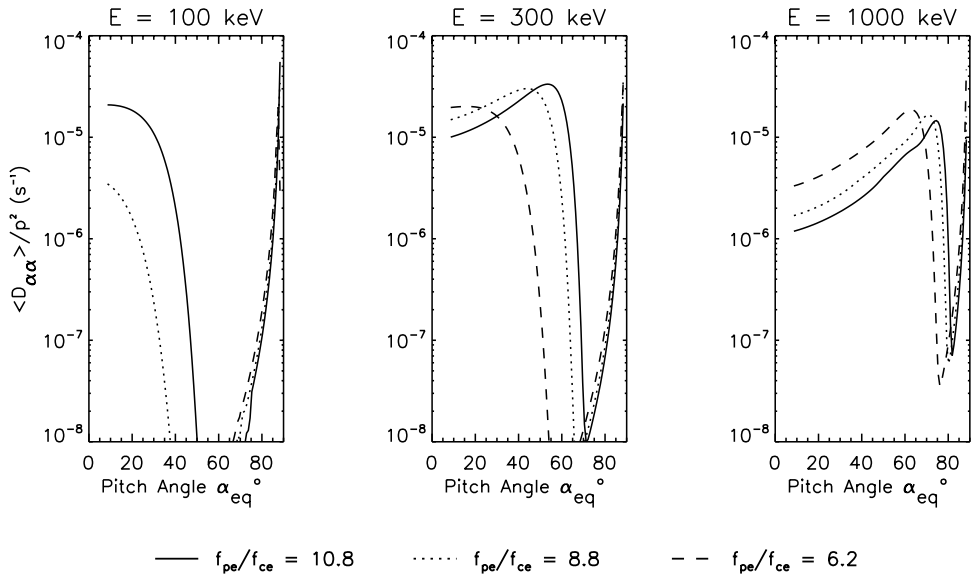

Figure 6. PADIE results for pitch angle diffusion coefficients at 100 keV, 300 keV, and 1 MeV due to plasmaspheric hiss, for a range of plasmaspheric density conditions equivalent to density levels of 1500 el.cm^{-3} (fpe/fce = 10.8), 1000 el.cm^{-3} (fpe/fce = 8.8), and 500 el.cm^{-3} (fpe/fce = 6.2) at L = 3.0. The edge of the loss cone is indicated by a vertical dot-dashed line.

[35] In Figure 4 we plotted the CRRES Neq results in comparison with the model of *Carpenter and Anderson* [1992] based on ISEE satellite data. The Carpenter and Anderson (C&A) model results for December at solar maximum agree reasonably well with the L = 2.5–4.0 CRRES Neq at American longitudes (−60°E). At higher *L*-shells the CRRES satellite observes lower density levels than the C&A model; this may possibly be due to the CRRES data including unsaturated plasmasphere conditions. In June at American longitudes (−60°E) the C&A model over estimates the electron density level consistently at all *L*-shells, and in December *L*-shells greater than L = 3.5 have consistently lower CRRES density levels than C&A. This appears to be in part because of the influence of some unsaturated plasmasphere Neq values in the CRRES data, and also because of the lack of a longitudinal component in the annual density variation of C&A.

[36] Using the PADIE code and holding all variables constant apart from the background electron density we find that hiss driven precipitation into the atmosphere will become spectrally harder at American longitudes as the season changes from December to June. At Asian longitudes there would be little change in the precipitation particle energy spectra with season. An additional influence of the changing background density in the plasmasphere could be on the generation and amplification of the hiss waves themselves. If the source of free energy to drive the waves remains the same, then reducing (increasing) the electron density should increase (decrease) the band of frequencies generated, affecting the resonant energies. So, although here we have shown that the annual changes in background electron density have an influence on the dynamics of radiation belt particles, the picture is far from complete and requires further study. Additionally, experimental evidence of this effect on the radiation belt particles has yet to be published.

7. Summary

[37] We have used CRRES measurements of plasmaspheric equatorial electron density at solar maximum to investigate the longitudinal and annual variation in density in the range L = 2.5–5.0. We find that the largest annual variation occurs at American longitudes (−60°E), and that no annual variation occurs at Asian longitudes (+100°E). These findings are in agreement with *Clilverd et al.* [1991]. The underlying cause is due to the influence of a tilted-offset dipole geomagnetic field. At American longitudes there is the largest discrepancy between geomagnetic latitude and geographic latitude. This leads to substantial annual variations in ionospheric plasma density, which map up into the plasmasphere as a consequence of diffusive equilibrium.

[38] Plasmaspheric electron density is larger in December than in June in the region covering −180°E to +20°E. Elsewhere the ratio of December to June is very close to 1.0. The annual variation also differs with *L*-shell. At American longitudes (−60°E), and possibly at New Zealand longitudes, the maximum December/June ratio is at L = 2.5–3.5, with a value of 2.7 at American longitudes at solar maximum. At L = 4.5 and above the annual variation disappears, possibly because the plasmasphere is not in diffusive equilibrium with the ionosphere at these high *L*-shells, or the inclusion of non-saturated electron density values from CRRES observations. The lowest electron density values for a given *L*-shell occur at American longitudes. This is particularly clear for the lower *L*-shells, although apparent as far out as L = 4.5. These values occur

in June. Clearly, the plasmasphere is strongly controlled by the configuration of the Earth's magnetic field and the annual variations in the F2 regions that are in diffusive equilibrium with it.

[39] Ion densities also show significant annual variations. There are similar longitudinal characteristics in the case of IMAGE EUV He^+ measurements taken during June and December 2001. However, there are as yet unexplained differences in atomic mass density measurements calculated using the magnetometer cross-phase technique, where European values are significantly higher than those at American longitudes and require a large correction factor for the ion composition.

[40] Calculations of the effect of changing plasmaspheric density on wave-particle interactions with plasmaspheric hiss indicate that the depletion of the plasmasphere at American longitudes in June results in a harder energy spectrum of electrons being precipitated into the atmosphere at those longitudes than anywhere else. Conversely, the softest energy spectrum occurs at the same longitudes in December. Little variation in precipitation energy spectrum is likely at Asian longitudes due to the absence of any significant annual variation in plasmaspheric density.

[41] **Acknowledgments.** Zuyin Pu thanks Dennis Gallagher and Ondrej Santolik for their assistance in evaluating this paper.

References

Anderson, R. R., D. A. Gurnett, and D. I. Odem (1992), CRRES Plasma-Wave Experiment, *J. Spacecr. Rockets*, *29*(4), 570–573.

Berube, D., M. B. Moldwin, and J. M. Weygand (2003), An automated method for the detection of field line resonance frequencies using ground magnetometer techniques, *J. Geophys. Res.*, *108*(A9), 1348, doi:10.1029/2002JA009737.

Carpenter, D. L., and R. R. Anderson (1992), An ISEE/whistler model of equatorial electron-density in the magnetosphere, *J. Geophys. Res.*, *97*, 1097–1108.

Chappell, C. R., K. K. Harris, and G. W. Sharp (1970), Morphology of bulge region of plasmasphere, *J. Geophys. Res.*, *75*, 3848–3861.

Clilverd, M. A., A. J. Smith, and N. R. Thomson (1991), The annual variation in quiet time plasmaspheric electron density determined from whistler mode group delays, *Planet. Space Sci.*, *39*, 1059–1067.

Clilverd, M. A., N. R. Thomson, and A. J. Smith (1992), Observation of two preferred propagation paths for VLF signals received at a non-conjugate location, *J. Atmos. Terr. Phys.*, *54*, 1075–1079.

Clilverd, M. A., et al. (2003), In situ and ground-based intercalibration measurements of plasma density at L = 2.5, *J. Geophys. Res.*, *108*(A10), 1365, doi:10.1029/2003JA009866.

Gallagher, D. L., M. L. Adrian, and M. W. Liemohn (2005), Origin and evolution of deep plasmaspheric notches, *J. Geophys. Res.*, *110*, A09201, doi:10.1029/2004JA010906.

Glauert, S. A., and R. B. Horne (2005), Calculation of pitch angle and energy diffusion coefficients with the PADIE code, *J. Geophys. Res.*, *110*, A04206, doi:10.1029/2004JA010851.

Guiter, S. M., C. E. Rasmussen, T. I. Gombosi, J. J. Sojka, and R. W. Shunk (1995), What is the source of observed annual variations in plasmaspheric density, *J. Geophys. Res.*, *100*, 8013–8020.

Gurnett, D. A., and R. R. Shaw (1973), Electromagnetic radiation trapped in the magnetosphere above the plasma frequency, *J. Geophys. Res.*, *78*, 8136–8149.

Helliwell, R. A. (1965), *Whistlers and Related Ionospheric Phenomena*, Stanford Univ. Press, Stanford, Calif.

Horne, R. B., S. A. Glauert, and R. M. Thorne (2003), Resonant diffusion of radiation belt electrons by whistler-mode chorus, *Geophys. Res. Lett.*, *30*(9), 1493, doi:10.1029/2003GL016963.

Lyons, L. R., R. M. Thorne, and C. F. Kennel (1972), Pitch angle diffusion of radiation belt electrons within plasmasphere, *J. Geophys. Res.*, *77*, 3455–3474.

Menk, F. W., D. Orr, M. A. Clilverd, A. J. Smith, C. L. Waters, and B. J. Fraser (1999), Monitoring spatial and temporal variations in the dayside plasmasphere using geomagnetic field line resonances, *J. Geophys. Res.*, *104*, 19,955–19,970.

Menk, F. W., C. L. Waters, and B. J. Fraser (2000), Field line resonances and waveguide modes at low latitudes: 1. Observations, *J. Geophys. Res.*, *105*, 7747–7761.

Meredith, N. P., R. B. Horne, R. M. Thorne, D. Summers, and R. R. Anderson (2004), Substorm dependence of plasmaspheric hiss, *J. Geophys. Res.*, *109*, A06209, doi:10.1029/2004JA010387.

Meredith, N. P., R. B. Horne, S. A. Glauert, R. M. Thorne, D. Summers, J. M. Albert, and R. R. Anderson (2006), Energetic outer zone electron loss timescales during low geomagnetic activity, *J. Geophys. Res.*, *111*, A05212, doi:10.1029/2005JA011516.

Olson, W. P., and K. Pfitzer (1977), Magnetospheric magnetic field modelling, *Annu. Sci. Rep. F44620-75-c-0033*, Air Force Off. of Sci. Res., Arlington, Va.

Orr, D., and J. A. D. Matthew (1971), The variation of geomagnetic micropulsation periods with latitude and the plasmapause, *Planet. Space Sci.*, *19*, 897–904.

Park, C. G., D. L. Carpenter, and D. B. Wiggin (1978), Electron density in the plasmasphere: whistler data on solar cycle, annual and diurnal variations, *J. Geophys. Res.*, *83*, 3137–3144.

Rasmussen, C. E., and R. W. Shunk (1990), A three-dimensional time-dependent model of the plasmasphere, *J. Geophys. Res.*, *95*, 6133–6144.

Richards, P. G., T. Chang, and R. H. Comfort (2000), On the causes of the annual variation in the plasmaspheric electron density, *J. Geophys. Res.*, *62*, 935–946.

Rippeth, Y., R. J. Moffett, and G. J. Bailey (1991), Model plasmasphere calculations for L-values near 2.5 at the longitude of Argentine Islands, Antarctica, *J. Atmos. Terr. Phys.*, *53*, 551–555.

Rozanov, E., L. Callis, M. Schlesinger, F. Yang, N. Andronova, and V. Zubov (2005), Atmospheric response to NO_y source due to energetic electron precipitation, *Geophys. Res. Lett.*, *32*, L14811, doi:10.1029/2005GL023041.

Sandel, B. R., R. A. King, W. T. Forrester, D. L. Gallagher, A. L. Broadfoot, and C. C. Curtis (2001), Initial results from the IMAGE extreme ultraviolet imager, *Geophys. Res. Lett.*, *28*, 1439–1442.

Sandel, B. R., J. Goldstein, D. L. Gallagher, and M. Spasojević (2003), Extreme ultraviolet imager observations of the structure and dynamics of the plasmasphere, *Space Sci. Rev.*, *109*, 25–46.

Saxton, J. M., and A. J. Smith (1989), Quiet time plasmaspheric electric fields and plasmasphere-ionosphere coupling fluxes at L = 2.5, *Planet. Space Sci.*, *37*, 283–293.

Singer, H. J., W. P. Sullivan, P. Anderson, F. Mozer, P. Harvey, J. Wygant, and W. McNeil (1992), Fluxgate magnetometer instrument on the CRRES, *J. Spacecr. Rockets*, *29*, 599–601.

Strangeways, H. J. (1991), The upper cutoff frequency of nose whistlers and implications for duct structure, *J. Atmos. Terr. Physics*, *53*, 151–169.

Sutcliffe, P. R., S. K. F. Hattingh, and H. F. V. Boshoff (1987), Longitudinal effects on the eigenfrequencies of low-latitude Pc3 pulsations, *J. Geophys. Res.*, *92*, 2535–2543.

Tarcsai, G., P. Szemeredy, and L. Hegymegi (1988), Average electron density profiles in the plasmasphere between L = 1.4–3.2 deduced from whistlers, *J. Atmos. Terr. Phys.*, *50*, 607–611.

Taylor, J. P. H., and A. D. M. Walker (1984), Accurate approximate formulae for toroidal standing hydromagnetic oscillations in a dipolar geomagnetic field, *Planet. Space Sci.*, *32*, 1119–1124.

Walker, A. D. M., J. M. Ruohoniemi, K. B. Baker, R. A. Greenwald, and J. C. Samson (1992), Spatial and temporal behaviour of ULF pulsations observed by the Goose Bay HF radar, *J. Geophys. Res.*, *97*, 12,187–12,202.

Waters, C. L., F. W. Menk, and B. J. Faser (1994), Low latitude geomagnetic field line resonance; experiment and modelling, *J. Geophys. Res.*, *99*, 17,547–17,558.

Webb, P. A., and E. A. Essex (2001), A dynamic diffusive equilibrium model of the ion densities along plasmaspheric magnetic flux tubes, *J. Atmos. Solar Terr. Phys.*, *63*, 1249–1260.

R. R. Anderson, Department of Physics and Astronomy, University of Iowa, Iowa City, IA 52242-1479, USA. (roger-r-anderson@uiowa.edu)

M. A. Clilverd, S. A. Glauert, R. B. Horne, and N. P. Meredith, British Antarctic Survey, Natural Environment Research Council, Madingley Road, Cambridge CB3 0ET, UK. (macl@bas.ac.uk; sagl@bas.ac.uk; rh@bas.ac.uk; nmer@bas.ac.uk)

F. M. Menk, Department of Physics, University of Newcastle, Callaghan, NSW 2308, Australia. (fred.menk@newcastle.edu.au)

B. R. Sandel, Lunar and Planetary Laboratory, University of Arizona, Sonett Space Sciences Building, 1541 East University Boulevard, Tucson, AZ 85711-0063, USA. (sandel@arizona.edu)

N. R. Thomson, Department of Physics, University of Otago, P. O. Box 56, Dunedin, New Zealand. (n_thomson@physics.otago.ac.nz)